Int. J. Heat Mass Transfer. Vol. 30, No. 12, pp. 2559–2570, 1987
Printed in Great Britain

0017 9310/87 $3.00 + 0.00

Double-diffusive flow and heat transfer for a cylindrical source submerged in a salt-stratified solution

D. G. NEILSON and F. P. INCROPERA
Heat Transfer Laboratory, School of Mechanical Engineering, Purdue University, West Lafayette, IN 47907, U.S.A.

(*Received* 4 *January* 1987 *and in final form* 30 *April* 1987)

Abstract—An experimental study has been performed to delineate the nature of double-diffusive flows induced by a heated horizontal cylinder submerged in a salt-stratified solution. Flow conditions depend strongly on a stratification parameter, N, which measures the initial degree of stable solute stratification relative to destabilizing thermal effects. For large N flow is initially confined to multiple recirculating fluid layers which exist around and above the heat source and are separated by diffusive interfaces. With increasing time the interfaces are eroded, causing merger of the convecting fluid layers and envelopment of the heat source by a single layer. With decreasing N, or in the later stages of an experiment for large N, conditions are strongly influenced by plume development above the cylinder. Flow in the convection layer about the cylinder is driven by the plume, which also enhances degradation of the diffusive interface separating the layer from the overlying fluid. For all values of N, steady-state conditions are only reached after the plume penetrates to the free surface and achievement of a uniform salt concentration eliminates the existence of double-diffusive effects. For a prescribed time the average cylinder Nusselt number decreases with increasing N. However, irrespective of N the Nusselt number increases with time to the limiting value associated with free convection in an unstratified, infinite medium.

INTRODUCTION

UNDER the influence of gravity, the presence of two diffusing species in a solution may result in double-diffusive convection. For this phenomenon to occur, the diffusing components must possess different molecular diffusivities and one of the components must be distributed in a hydrostatically unstable manner. Differential diffusion is then responsible for the development of local density anomalies which, in turn, induce buoyancy driven convection.

A common form of double-diffusive convection occurs when a solutally stratified fluid is thermally destabilized, inducing a complex pattern of convecting and non-convecting fluid layers. The occurrence of such phenomena in geophysical flows [1] and in engineering applications such as crystal growth [2] and metal casting [3] has spawned numerous studies of convection in solutally stratified solutions which are uniformly heated from below [4]. Much less attention, however, has been given to the problem of non-uniform heating by discrete sources.

It is useful to contrast flows which occur when thermally stratified fluid is destabilized by localized heating with those which occur in a solutally stratified fluid. Experimental and theoretical treatments of the problem for thermally stratified enclosures [5, 6] indicate that, unlike natural convection in an unstratified medium, vertical development of the plume above a discrete, planar heat source is restrained by the stratification. As the ascending plume intrudes into an ambient which is increasingly hotter, its positive buoyancy decreases and an equilibrium level is reached. As shown in Fig. 1(a), excess momentum of the plume causes this level to exceed the point of neutral buoyancy. Because vertical growth is impeded, denser fluid at the apex of the plume moves downward and horizontally, as it seeks a stable level. The hori-

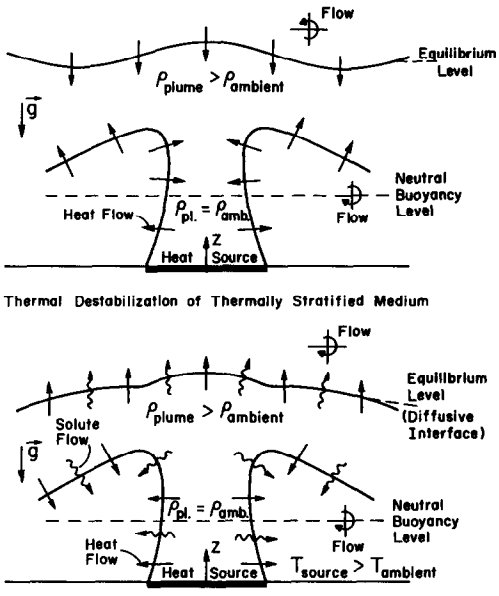

FIG. 1. Comparison of plume development above a discrete heat source in (a) thermally and (b) solutally stratified fluids.

NOMENCLATURE

A_s	cylinder surface area	Ra	thermal Rayleigh number, equation (2)
D	cylinder diameter	T_s	average cylinder surface temperature
g	gravitational acceleration	T_∞	ambient temperature
k	thermal conductivity	z	distance measured from test cell bottom.
Le	Lewis number, α/v		
m_s	salt mass fraction	Greek symbols	
N	stratification parameter, equation (3)	α	thermal diffusivity
$\overline{Nu}$	average Nusselt number, equation (1)	β_s	saline expansion coefficient
$\overline{Nu}^*$	normalized Nusselt number, $\overline{Nu}/\overline{Nu}_0$	β_T	thermal expansion coefficient
$\overline{Nu}_0$	reference Nusselt number, equation (4)	v	kinematic viscosity.
P	heater power		

zontal motion results in recirculating zones, which extend from both sides of the warm plume to the enclosure sidewalls. The horizontal motion also induces shear forces which drive counterrotating cells above the primary recirculating zones. Such effects have also been observed when heating is due to submerged cylindrical and spherical sources [7]. Moreover, for intense thermal stratification, plume development is eliminated, and buoyancy induced motion occurs exclusively in the horizontal direction. With increasing stratification horizontal motion originates at successively lower locations on the heat source and recirculation is confined to a single zone on each side of the source.

Conditions characterizing thermal plume development in an isothermal, solutally stratified medium are shown in Fig. 1(b). Aside from the basic shape of the plumes, there is little similarity with the conditions of Fig. 1(a). If the plume rises in a thermally stratified ambient, the direction of lateral heat transfer is reversed. However, no such reversal occurs for the solutally stratified case. Additional differences relate to conditions at the equilibrium level. In Fig. 1(a) heat flow is downward, thereby preserving the stability of the overlying fluid. In Fig. 1(b), however, heat flow is upward, and the equilibrium level corresponds to a double-diffusive interface, above which fluid may be destabilized and additional interfaces formed [8]. Moreover, since conditions are characterized by species transfer from the solute-rich plume to the ambient fluid, upward diffusion of heat and salt from the equilibrium level would decrease density differences between the plume and the overlying fluid, thereby eroding the existing interface and allowing new interfaces to be formed. It follows that, in an enclosure, steady conditions would only be achieved when the solution becomes totally mixed. A final distinction relates to the fact that, while flow above the equilibrium level of Fig. 1(a) is shear driven, flow above a double-diffusive interface is buoyancy driven.

Features delineated in Fig. 1(b) have been revealed in experimental and theoretical studies of a linearly salt-stratified solution heated by both a discrete strip in an otherwise adiabatic bottom [9, 10] and a small spherical source [11–13]. Pronounced double-diffusive layering is associated with heating by the spherical source, and three types of layers have been identified [13]. Type I layers, which are the last to develop, form above the basic plume structure (the diffusive interface shown in Fig. 1(b)). Heat transfer from the interface to the overlying fluid, which decreases with distance from the apex of the plume, induces vertical and horizontal temperature gradients and, hence, buoyancy drive fluid motion. In contrast, Type II layers develop in a vertical region corresponding to the top one-third of the plume. The horizontal temperature difference between the warm plume and the cooler ambient generates horizontal cellular growth much like that which has been observed for sidewall heating [14]. Type III layers form around the lower part of the rising plume and are driven by the same mechanism as Type II layers. However, Type III layers contain warmer and more saline solution originating from the source. As the layers grow laterally, they become more dense due to heat loss to the cooler ambient and the diffusive interfaces slope downward.

Within a Type II or III layer, flow is characterized by warm, solute-rich fluid moving away from the plume at the top of the layer and cool, solute-depleted fluid moving toward the plume at the bottom of the layer. Vorticity within the layer is created by the positive buoyancy and the large horizontal velocity gradients experienced by fluid approaching the plume at the bottom of the layer. It is maintained by shear forces and non-uniform cooling experienced by fluid leaving the plume. Thermal and solutal conditions within a layer may also induce a finger-like convection pattern [1], particularly for Type III layers.

Experimental studies have also been performed for an isothermal cylinder submerged in a salt-stratified solution [15, 16]. Although detailed features of the double-diffusive flows are not delineated, measurements were performed to determine the effects of stratification on convection heat transfer from the cylinder. The results indicate that, for a prescribed thermal Rayleigh number, the average cylinder Nus-

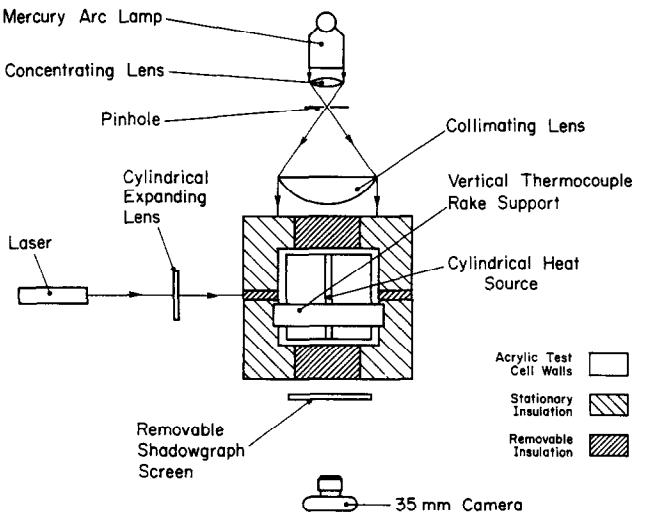

FIG. 2. Top view of test cell and optical systems.

selt number is substantially reduced by the stratification.

The purpose of the present study has been to extend the foregoing work by obtaining an improved understanding of double-diffusive flows induced by a cylindrical heat source in a salt-stratified solution. Flow details have been established for a wide range of operating conditions and have been used as a basis for interpreting convection heat transfer measurements.

EXPERIMENTAL PROCEDURES

A top view of the experimental system is shown schematically in Fig. 2. The test cell measures 305 mm on a side, with sidewalls fabricated from 25.4 mm thick clear acrylic. Holes, 25.4 mm in diameter and centered 38.1 mm from the bottom, were drilled in two of the opposing sidewalls to support the cylindrical heat source. The bottom of the test cell consisted of a 3.18 mm thick copper plate, which was separated from a guard heater by a 50.8 mm thick layer of styrofoam insulation. The heater was used to eliminate heat losses through the bottom. The test cell walls were covered with 50.8 mm thick styrofoam insulation, and to suppress evaporation, the top of the test cell was covered with a 1.6 mm thick acrylic sheet.

The 305 mm long cylindrical heat source consisted of a 25.4 mm diameter copper rod (Fig. 3), with a cartridge heater inserted through a 6.35 mm diameter hole. Power dissipation in the connecting leads and heat loss through the cylinder end supports were negligible. Temperatures at the outer surface of the cylinder were measured with copper–constantan thermocouples inserted in twelve 0.330×0.635 mm grooves, spaced at 30° intervals around the cir-

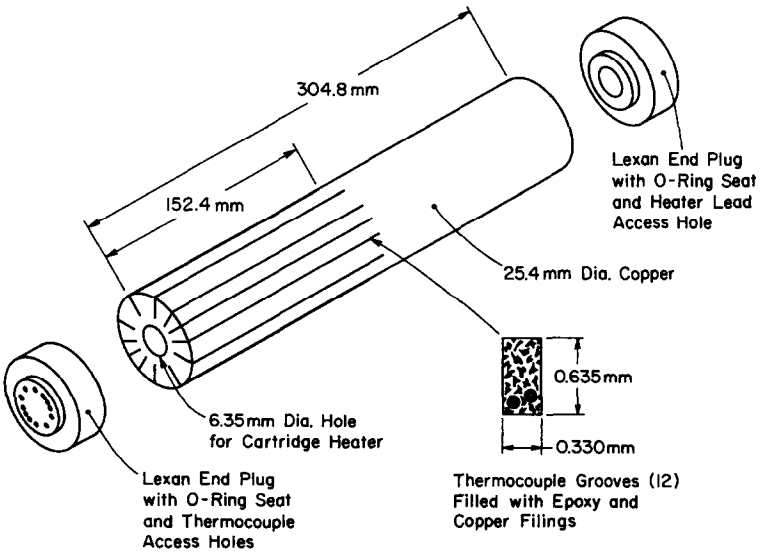

FIG. 3. Schematic of heated cylinder.

Table 1. Conditions for experiments with salt-stratified solutions

Experiment	dm_s/dz (% m^{-1})	ΔT_{max} (°C)	N	Ra (10^6)
1	16.9	4.9	3.0	1.37
2	17.4	4.8	2.9	1.46
3	14.8	4.7	2.2	1.72
4	12.2	5.1	1.7	1.92
5	11.8	6.8	1.2	3.40
6	12.0	9.6	0.95	3.62
7	15.6	13.6	0.81	6.51
8	5.6	9.9	0.46	3.94
9	4.3	10.4	0.31	5.01
10	3.4	22.7	0.12	10.86

cumference. The grooves were filled with a conductive, copper filled epoxy, and for the experimental conditions temperature measurements revealed differences of less than 0.2°C around the circumference. Hence, the cylinder was assumed to be isothermal at a temperature corresponding to the average of the 12 readings. To protect it from the saline environment, the cylinder was coated with a 0.025 mm layer of phenolic polytetrafluoroethylene, and a small surface temperature correction was made to account for the thermal resistance of the layer.

Following the start of heating, an average Nusselt number was calculated from the expression

$$\overline{Nu} = \frac{(P/A_s)D}{k(T_s - T_\infty)} \tag{1}$$

where the ambient temperature was measured on one sidewall at a height of 38 mm. Since the average surface and ambient temperatures increased with time during the experiments, the thermal energy stored by the cylinder also increased with time. However, since the effect was small for all but a brief start-up, it was neglected in the data reduction. Each experiment was characterized in terms of a thermal Rayleigh number of the form

$$Ra = \frac{g\beta_T(T_s - T_\infty)_{max}D^3}{\alpha\nu} \tag{2}$$

where $(T_s - T_\infty)_{max}$ is the maximum temperature difference recorded during the experiment. Thermophysical properties in equations (1) and (2) were evaluated at the arithmetic mean of the surface and ambient temperatures and at the initial salt concentration for the cylinder midheight [17].

A linear salinity profile was established by using the double-bucket technique [14] to continuously introduce a progressively saltier solution into the bottom of the test cell. Confirmation of a linear gradient was obtained by extracting 2 ml samples at various depths in the test cell and performing a weight analysis. The degree of stable stratification (relative to the destabilizing thermal buoyancy) was quantified in terms of the parameter

$$N = -\frac{\beta_s(dm_s/dz)D}{\beta_T(T_s - T_\infty)_{max}} \tag{3}$$

where dm_s/dz is the initial gradient of the salt mass fraction. In the order of decreasing N, the experimental conditions are summarized in Table 1.

Two thermocouple rakes were used to monitor vertical temperature distributions in the salt solution. One rake contained 24 copper–constantan thermocouples and was positioned 70 mm from the centerline of the cylinder, while the other rake contained eight thermocouples and was stationed at one of the sidewalls.

Flow visualization was performed using the shadowgraph imaging technique (Fig. 2). A collimated beam of white light was passed through the test cell, and the refracted image was photographed on a diffusing glass screen. In selected cases, the flow was also observed by passing the 1 mm diameter beam of a 100 mW argon ion laser through a 3 mm cylindrical glass lens. The resulting sheet of light was used to illuminate a thin vertical section of the test cell, into which fluorescein disodium dye was injected. When using the shadowgraph and fluorescent dye techniques, the sidewall insulation panels were removed to photograph the flow.

RESULTS

Flow visualization

Conditions for which stratification effects are most pronounced are shown in the shadowgraphs of Fig. 4. A thermocouple rake, the heater lead wires, and a centimeter scale appear to the left, bottom, and right, respectively, of each shadowgraph. Most evident is the fact that, unlike conditions in an unstratified medium [18], there is total suppression of plume development above the heated cylinder. Initial flow development corresponds to a small disturbance at the top of the cylinder and symmetric boundary layer growth at the bottom of the cylinder (Figs. 4(a) and (b)). However, as the solute-rich boundary layer fluid ascends along the bottom of the cylinder, its density becomes progressively larger than that of the ambient. Sustained vertical motion is therefore inhibited by a negative buoyancy force, and the boundary layer is deflected horizontally. Since the Lewis number is large ($Le \approx 80$), density differences between the boundary layer and ambient fluid are augmented by the differential diffusion rates of heat and salt. Hence, the boundary layer fluid begins to descend, as it cools rapidly while retaining most of its salt. Just below the bottom of the cylinder, the descending flow experiences a horizontal shear force produced by ambient fluid that is drawn to the heat source to replenish the boundary layer. The net effect is to create a symmetric vortex pair about the bottom of the cylinder (Fig. 4(c)). The vortex pair has also been revealed by visu-

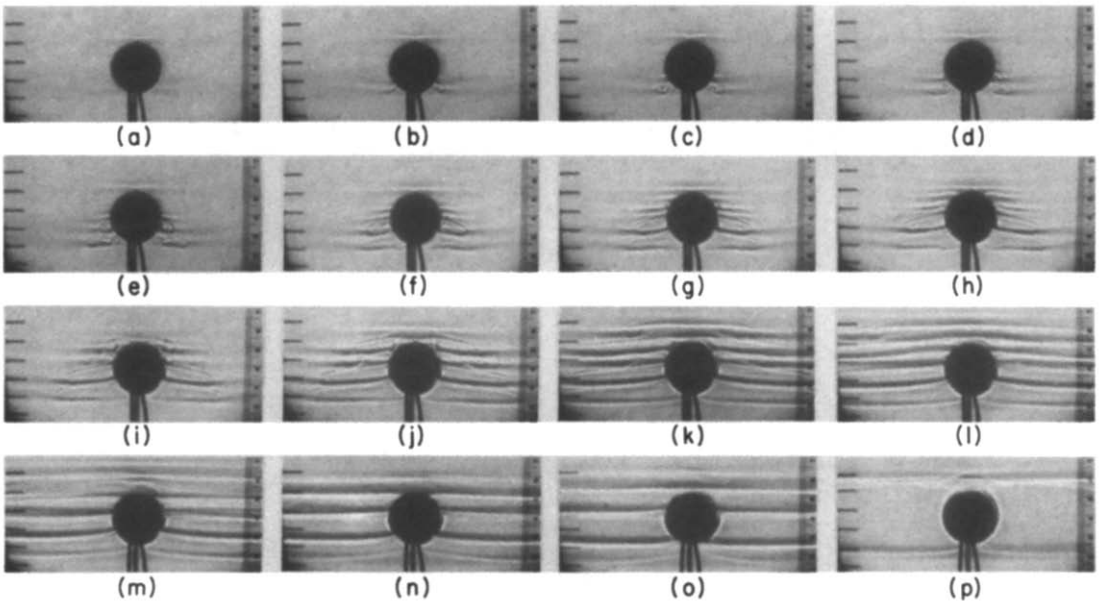

FIG. 4. Shadowgraphs of Experiment 1 ($N = 3.0$, $Ra = 1.37 \times 10^6$): (a) $t = 2.5$ min, (b) 3.7 min, (c) 4.3 min, (d) 5 min, (e) 6 min, (f) 8 min, (g) 10 min, (h) 11.5 min, (i) 13 min, (j) 18 min, (k) 26 min, (l) 35 min, (m) 50 min, (n) 1.5 h, (o) 2.5 h, (p) 14 h.

alizing fluorescein dye injected at the bottom of the heated cylinder.

The foregoing process is replicated in a second boundary layer region which develops above the first region (Figs. 4(d) and (f)). However, although formation of the second vortex pair is determined by mechanisms equivalent to those which drive the first pair, restoration of ascending flow in the second pair is enhanced by vertical heat transfer from the lower vortices. Similar processes characterize the formation of third and fourth boundary layer regions (Figs. 4(f)–(i)).

Horizontal propagation of the convection layers is evident in Fig. 4(j). Regions separated by diffusive interfaces (dark bands) correspond to four convection layers on each side of the isothermal heat source. All layers are of the Type III category reported by Tsinober *et al.* [13]. Flow in each layer is driven primarily by the heated cylinder and is analogous to flow observed for sidewall heating of a stable solute gradient [14]. The gentle, downward slope of the interfaces is due to heat transfer from the warmer fluid below an interface to cooler fluid above the interface.

The changing nature of the subsequent flow is revealed by Figs. 4(k)–(p). The third convection layer (from the bottom) thickens and moves vertically upward, while thermally unstable conditions due to heat transfer from the fourth layer result in formation of a fifth layer (Figs. 4(k) and (l)). Subsequent erosion of the diffusive interface separating the fourth and fifth layers, and hence merger of the layers (Figs. 4(l) and (m)), is consistent with observations for mixed layer development due to uniform bottom heating [8]. The thickness of the second layer also expands, with subsequent erosion of interfaces associated with the fourth, third and first layers leaving a single well-mixed layer around the heated cylinder (Fig. 4(p)). Although the experiment was terminated after 14 h, continued heating would have caused slow expansion of the upper diffusive interface, until well-mixed conditions were achieved throughout the test cell.

The foregoing trends were also revealed in Experiments 2–4, although, with decreasing N, fewer convection layers formed around the cylinder during the early stages of heating. The increased thickness of these layers is consistent with results obtained for sidewall heating [14]. Vertical temperature scans obtained during the experiments revealed the existence of a slightly positive vertical temperature gradient in the convection layers and large positive temperature gradients across the diffusive interfaces.

For $N \lesssim 1$, flow development is characterized by a single convection layer around the heated cylinder. Representative results from Experiment 6 are shown in Fig. 5. Shortly after the onset of heating, a small plume forms at the top of the cylinder (Fig. 5(a)). However, plume development is inhibited by the stable concentration gradient, and a diffusive interface is established (Fig. 5(b)). Formation of the small vortices at the horizontal extremes of this interface is initiated by heat transfer from the upper and lower regions of the laterally spreading plume. The attendant negative buoyancy induces downward motion, and the cooled, solute-rich plume overshoots the point of neutral buoyancy. Heat transfer from the warmer ambient and shear effects subsequently cause the fluid

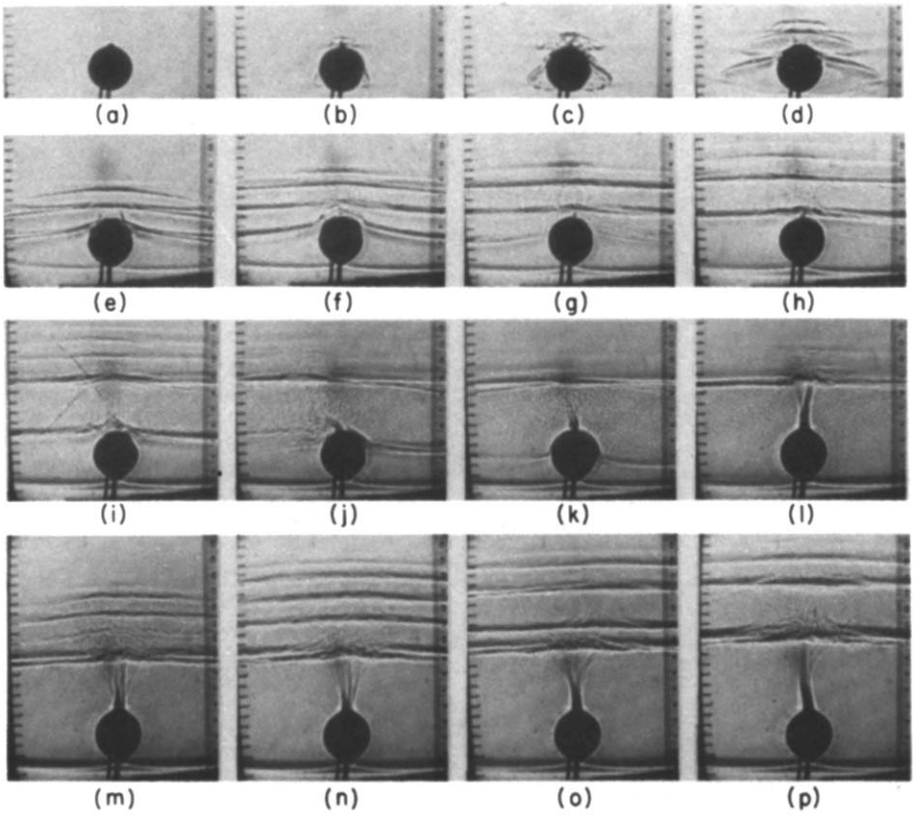

FIG. 5. Shadowgraphs of Experiment 6 ($N = 0.95$, $Ra = 3.62 \times 10^6$): (a) $t = 30$ s, (b) 1 min, (c) 2 min, (d) 4 min, (e) 9 min, (f) 18 min, (g) 35 min, (h) 1.2 h, (i) 2.75 h, (j) 3.2 h, (k) 3.3 h, (l) 3.5 h, (m) 3.8 h, (n) 4.2 h, (o) 5.5 h, (p) 6.2 h.

to ascend and the vortex pair is formed. The magnitude of the vorticity is sufficient to induce the vigorous mixing indicated by Fig. 5(c).

A second vortex pair results from boundary layer development at the bottom of the cylinder (Figs. 5(b) and (c)). Although the flow is typical of that observed for larger values of N, the boundary layer detaches from the cylinder at a higher level (close to the top). The increased thermal buoyancy draws salt laden solution from the lower portion of the cylinder, causing enhanced sloping of the diffusive interface as the cell cools.

Both of the foregoing vortex pairs yield developing convection layers, one around and the other above the cylinder. Moreover, upward heat flow from the top layer induces a third convection zone (Fig. 5(d)). This heat flow, which is a maximum at the apex of the plume and decreases along the interface, induces a destabilizing temperature gradient in the overlying fluid. Buoyancy induced motion follows onset of the instability, while restrictions imposed by the stabilizing salinity gradient cause a new diffusive interface to be established. The existence of a three tier pattern of convection layers is evident in Fig. 5(e). Convection in the lowermost (Type III) layer, which envelops the cylinder, is driven by the cylinder thermal boundary layer, while convection in the second (Type II) layer is driven by the plume ascending from the cylinder. The second layer is classified as Type II, since motion is driven by the horizontal temperature gradient between the central plume and the ambient fluid and does not originate from the lower portion of the heat source. The top layer is classified as Type I, since motion is driven by non-uniform heating along its bottom interface.

With increasing time the diffusive interface separating the lower convective layers begins to erode (Figs. 5(f) and (g)), and fluid from the bottom layer penetrates into the second layer. This intrusion of saltier fluid depresses the interface and, by increasing the density of the second layer, enhances erosion of the interface, creating a single, well-mixed layer about the cylinder (Fig. 5(h)). Aside from the development of weak convection layers above the second (previously the third) mixed layer and slow growth of the second layer, there is little change in flow conditions during the next 1.5 h.

Two hours and forty-five minutes into heating, wisps of warm fluid emanating from the cylinder penetrate the overlying diffusive interface (Fig. 5(i)). The wisps convect heavier fluid from the first to the second layer, thereby increasing the density of the second layer and eroding the intervening interface (Figs. 5(j) and (k)). In addition, interfaces above the second layer also decay, implying that heat transfer from the second layer is insufficient to sustain convective

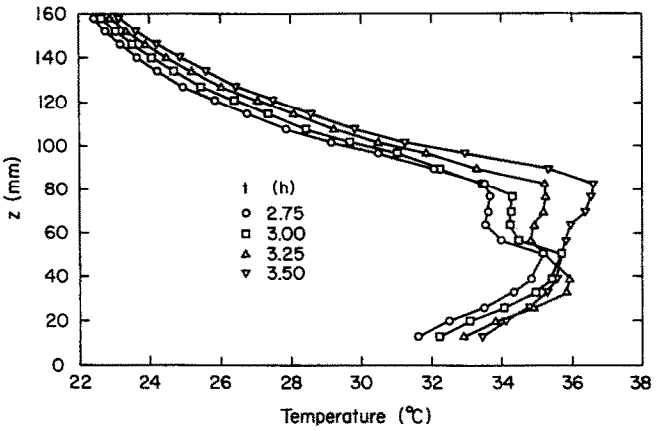

FIG. 6. Vertical temperature distributions during layer merger for Experiment 6.

motion. Hence, during this period, the plume's thermal energy is used primarily to establish well-mixed conditions in a large bottom layer (Fig. 5(l)).

Figure 6 shows vertical temperature distributions, taken approximately 70 mm from the heat source, during merger of the lower mixed layers. Initially, the layer around the cylinder is characterized by a temperature profile which is typical of a recirculating cell formed by a horizontal temperature gradient. The upper region of the cell at approximately 50 mm contains warm fluid propagating away from the cylinder, and the bottom of the cell at 25 mm consists of cooler fluid moving toward the heated cylinder. Conditions within the overlying recirculating cell (55–85 mm) are similar, although much less pronounced, since upward heat flow from the bottom cell creates a more uniform temperature profile. As time progresses, the temperature (and salinity) difference between the two layers diminishes, and a single recirculating layer is formed (Fig. 5(l)).

Multiple mixed layers again form above the lower layer due to heat transfer from the plume impinging on the top interface of the bottom layer (Figs. 5(m) and (n)). However, erosion of the interface between the second and third layers results in merger of the two layers (Figs. 5(o) and (p)), and had the experiment been continued, the top interface of the bottom layer would have subsequently been eroded. Temperature measurements corresponding to the conditions of Fig. 5(p) yielded a slightly increasing temperature with increasing elevation in each of the mixed layers. Such a variation again indicates a recirculation pattern in which warm fluid propagates toward the sidewall at the top of a layer and away from the sidewall at the bottom.

The effects of further reducing the stratification parameter are revealed in Fig. 7. Unlike results obtained for larger values of N, the buoyant upflow, which develops at the bottom of the heat source, has sufficient momentum to rise above the isothermal cylinder (Fig. 7(a)). However, ascension of this flow is impeded by the decreasing ambient density and a vortex cap is soon formed (Fig. 7(b)). The differential diffusion of heat and salt is then responsible for a nearly vertical descent of the salt-rich fluid. The shear gradient between the rising plume and the cooling downflow generates vorticity, which leads to the counter-rotating vortex pair shown in Fig. 7(c). Subsequently, the ascending plume interacts with the vortex pair and part of the upflow is forced laterally (Fig. 7(d)). As this portion of the flow cools, it descends around the heat source (Fig. 7(e)), while enhanced penetration (or re-emergence) of the plume into the overlying stable region also occurs. Vigorous mixing results from the combined effect of the ascending plume and the adjoining downflow (Fig. 7(f)), and a diffusive interface begins to form at the top of the buoyant upflow (Fig. 7(g)). Fluid above this interface is destabilized by heat transfer from the interface (Fig. 7(g) and (h)), with the vertical heat flux being largest near the plume and decreasing in the horizontal direction. At $t = 3.5$ min (Fig. 7(h)), there are then two interfaces, with convective layers developing between the interfaces and between the lower interface and the heat source. Subsequently, additional interfaces develop above the second interface and below the heat source (Figs. 7(i) and (j)), creating three well-mixed fluid layers. Since the image produced by the shadowgraph is an integration of flow conditions across the test chamber, bifurcation of the plume (Fig. 7(j)) indicates three-dimensional plume behavior due to variations in the axial direction.

Using the fluorescein dye technique, two distinct flow conditions were observed to exist in the layer extending from the bottom of the heat source to the first interface (Fig. 7(j)). The primary flow was driven by horizontal temperature gradients and consisted of a global recirculation for which warm, salty fluid moved toward the sidewalls in upper regions of the layer, while cooler fresher water moved away from the sidewall in lower regions. In addition, the existence of warm, salty fluid over cooler, fresher fluid induced a *finger* instability [1], for which convection due to descending salt fingers was superimposed on the recir-

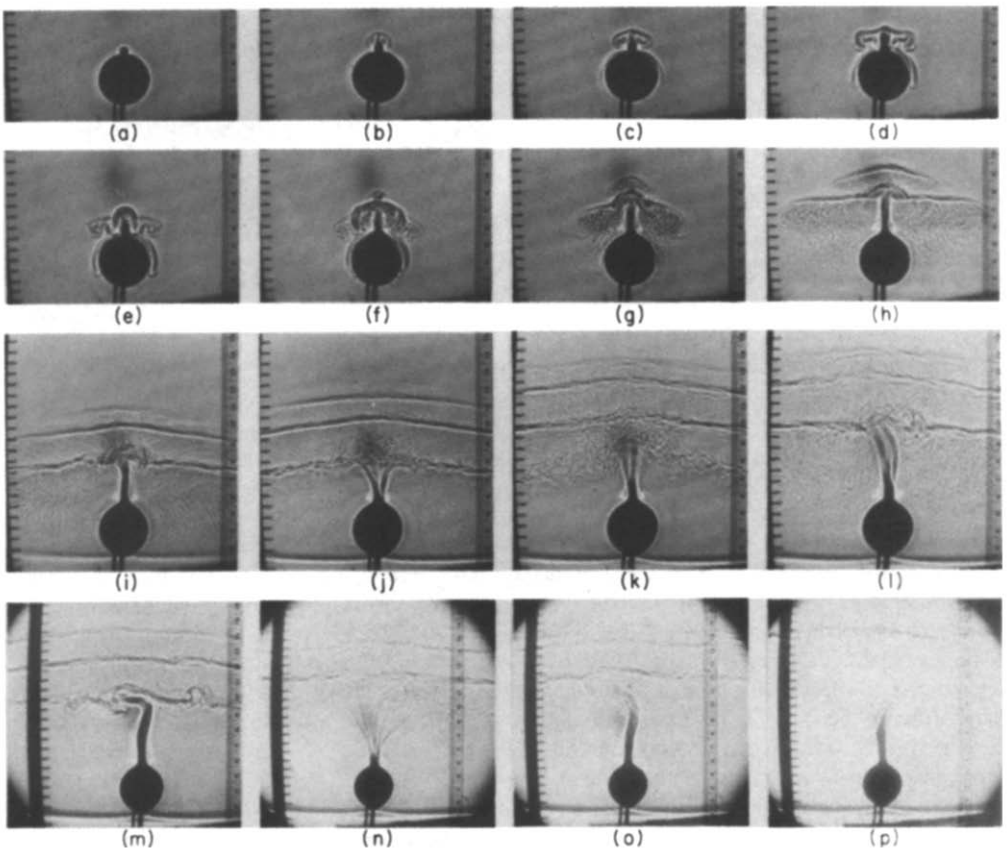

FIG. 7. Shadowgraphs of Experiment 9 ($N = 0.31$, $Ra = 5.01 \times 10^6$): (a) $t = 30$ s, (b) 37 s, (c) 45 s, (d) 1 min, (e) 1.1 min, (f) 1.5 min, (g) 2 min, (h) 3.5 min, (i) 8 min, (j) 15 min, (k) 28 min, (l) = 36 min, (m) 50 min, (n) 1.2 h, (o) 1.75 h, (p) 3 h.

culating flow. Hence, conditions were characterized by the co-existence of both forms of double-diffusive convection [1], namely diffusive layering and solutal fingers. The effect of the *finger* instability became less pronounced with increasing time, as the convecting layer produced a well-mixed salinity condition. Such phenomena have also been observed for point heat sources [13].

With increasing time, there is erosion of the first diffusive interface above the cylinder and, as warm, salty fluid from the bottom mixed layer intrudes into the overlying layer, there is merger of the two layers (Figs. 7(j)–(l)). Subsequently, transverse plume oscillations vigorously erode the next diffusive interface, as fluid is entrained from the overlying mixed layer into the bottom layer (Figs. 7(m)–(o)). The process continues with degradation of the next interface, until a single bottom mixed layer is separated from the stratified fluid by a single interface (Fig. 7(p)).

Results obtained for the weakest stratification level are shown in Fig. 8. Consistent with trends noted for decreasing N, a plume forms at the start of heating and ascends to a much higher level than that of the previous experiment. Rapid, vigorous mixing results as the impeded flow descends into the stable ambient, and a well-mixed bottom layer is formed within approximately 5 min (Fig. 8(i)). Multiple layer formation above the basic plume also occurs during the initial stages of heating. However, these layers quickly coalesce due to vigorous plume induced mixing, and after 20 min plume penetration approaches the free surface.

For all of the experiments, conditions beneath the heated cylinder were independent of changes in N and Ra. Although this region is characterized by stable thermal and solutal gradients, a weak flow is induced by shear forces acting along the diffusive interface attached to the bottom of the heat source. The motion could not be discerned in the shadowgraphs, but dye injection suggested the existence of a pair of weak, counter-rotating cells.

Heat transfer

To validate the measurement procedures and to provide a standard for assessing the effects of stratification, additional experiments were performed for pure, unstratified water and Rayleigh numbers in the range $4.5 \times 10^5 \leqslant Ra \leqslant 2.9 \times 10^6$. In each case, a limiting value of the average Nusselt number was reached and the result was within 2% of the following correlation for an isothermal cylinder in an infinite,

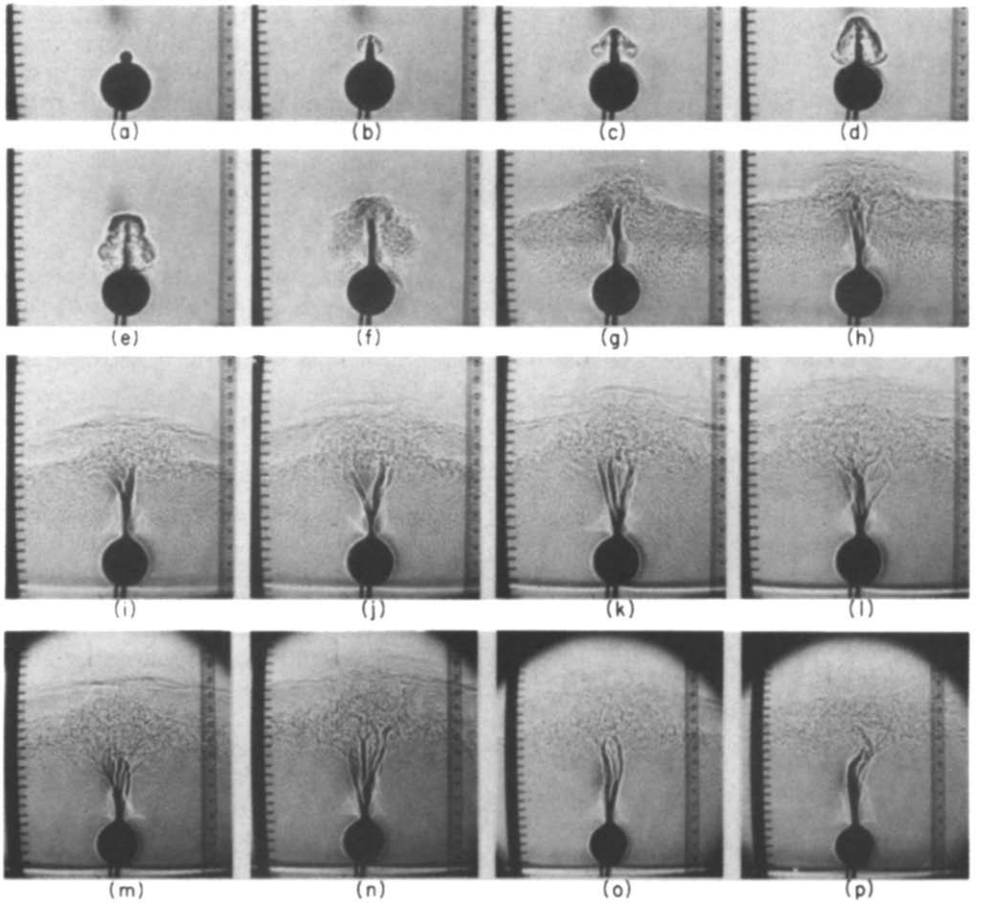

FIG. 8. Shadowgraphs of Experiment 10 ($N = 0.12$, $Ra = 10.86 \times 10^6$): (a) $t = 20$ s, (b) 27 s, (c) 33 s, (d) 40 s, (e) 48 s, (f) 1 min, (g) 2 min, (h) 3 min, (i) 5 min, (j) 6 min, (k) 8 min, (l) 10 min, (m) 12 min, (n) 14 min, (o) 16 min, (p) 19 min.

quiescent fluid [19]

$$\overline{Nu}_0 = 0.48 Ra^{1/4}, \quad 10^4 < Ra < 10^7. \qquad (4)$$

Agreement of the data with the foregoing correlation also suggests that finite cavity geometry effects are negligible.

The effect of solute stratification is revealed in Fig. 9, where normalized Nusselt number data are plotted as a function of time for experiments corresponding to $N = 0$, 0.95, and 2.2. In each case the sharp, initial decay in $\overline{Nu}^*$ is due to start-up heating of the cylinder wall, and not to hydrodynamic conditions. For $N = 0$, $\overline{Nu}^*$ recovers from this initial transient and is within 2% of the accepted limit after 1 h of heating.

The effects of solute stratification are revealed by contrasting Figs. 9(a) and (c). As expected, severe stratification inhibits buoyancy driven flows around the cylinder, markedly reducing $\overline{Nu}$ relative to that for an unstratified medium. As shown in Fig. 9(c), however, $\overline{Nu}^*$ ultimately increases, as double-diffusive effects promote the formation and growth of a single well-mixed convection layer around the cylinder. Before this condition is achieved ($t \lesssim 800$ min), development and subsequent erosion of multiple interfaces around the cylinder cause frequent and large temporal excursions in $\overline{Nu}^*$. In particular, changing hydrodynamic conditions due to multiple mixed layer development and coalescence affect the mean cylinder surface temperature, as well as the ambient temperature. For $t \gtrsim 800$ min, $\overline{Nu}^*$ continues to increase, with the sharp rise corresponding to upward propagation of the diffusive interface above the cylinder. This interface would propagate to the free surface and $\overline{Nu}^*$ would approach unity if the experiment were taken to completion.

The approach to conditions for an infinite, unstratified medium is revealed by the results of Fig. 9(b), where $\overline{Nu}^* \to 1$ for $t \gtrsim 400$ min. Depressions in $\overline{Nu}^*$ at 50, 210, 280, 325 and 375 min correspond to successive mergers of the lowermost convective layer with overlying layers. During coalescence, the ambient temperature decreases as the warm bottom layer mixes with the overlying cooler layer. Thus, the temperature difference between the heated cylinder and the ambient increases, causing $\overline{Nu}^*$ to decrease. The effect becomes less pronounced as the thermal capacitance of the bottom layer increases with each merger. In contrast, the interval from 60 to 140 min is char-

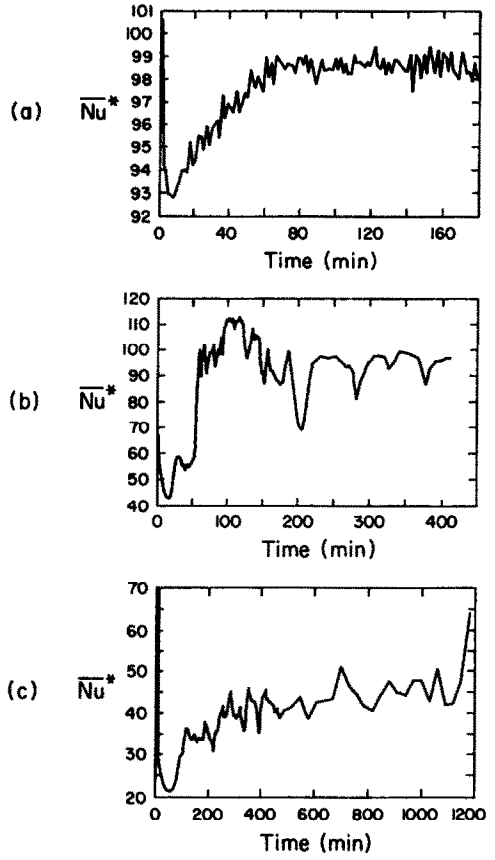

FIG. 9. Time dependence of normalized cylinder Nusselt number for (a) $N = 0$, (b) $N = 0.95$, and (c) $N = 2.2$.

acterized by a significant increase in $\overline{Nu}^*$. During this period, an interface remains attached to the top of the heated cylinder, while fluid from the bottom layer escapes into the overlying region (revealed by thermal wisps in Figs. 5(h) and (i)). The subsequent reduction in the height of the interface increases the temperature of fluid in upper regions of the bottom convective layer, thereby increasing the reference (ambient) temperature and the value of $\overline{Nu}^*$.

For Experiment 6, $\overline{Nu}$ achieved a value within 3% of equation (4) before the plume reached the free surface of the test cell (Fig. 5(p)). Similar results were obtained in Experiments 7–10, and in all cases good agreement with the infinite medium correlation was achieved when the plume height reached approximately 50 mm (two cylinder diameters). This result is consistent with the observations of previous investigators [15, 16].

The extent to which heat transfer is suppressed by solute stratification is revealed by plotting the minimum value of $\overline{Nu}^*$ as a function of N. The data of this study are plotted in Fig. 10, along with the results of Gebhart and Hubbell [15]. The data sets are in good agreement and reveal an approximately 75% reduction in $\overline{Nu}^*$ for $N > 2.2$. The adverse effect of solute stratification is associated with confinement of heat rejected by the cylinder to adjoining convection to layers. Heat rejection from these layers is limited by their ability to transfer energy across diffusive interfaces. In contrast, for natural convection without stratification, heat rejection is enhanced by dissipation of an ascending plume in an infinite medium.

The foregoing decrease in convective transfer differs markedly from results obtained for a thermally stratified medium [7]. A steepness parameter, which is defined as the ratio of stabilizing to destabilizing temperature differences, was used to assess the influence of thermal stratification on convection transfer from an isothermal cylinder. For increasing steepness, hydrodynamic conditions were similar to those observed with increasing N. That is, vertical plume growth was restrained, and for large steepness, growth was entirely horizontal. However, with increasing steepness, convection heat transfer was enhanced rather than suppressed.

SUMMARY

Double-diffusive convection, which is induced when two diffusing species make opposing contributions to the mass density, significantly influences hydrodynamic conditions around a cylindrical heat source. With the onset of heating, the nature of the

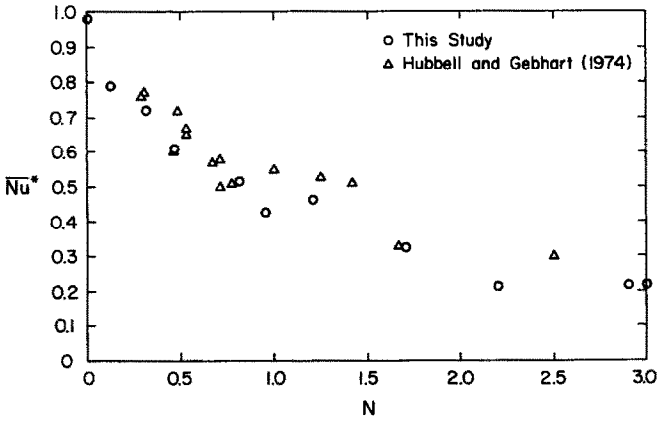

FIG. 10. Normalized minimum Nusselt number as a function of the stratification parameter.

flow depends strongly on the magnitude of N, which is a measure of the stabilizing solute gradient relative to destabilizing thermal effects associated with the heated cylinder. For large values of N, conditions are characterized by the development of multiple convection layers around the heated cylinder. The layers are separated by diffusive interfaces, and the recirculating flow within each layer is driven by the horizontal temperature gradient between the cylinder and the ambient. During the early stages of development, recirculation is confined to vortex pairs, while in subsequent stages salt fingers may be superposed on a recirculating flow. Eventually, gradual erosion of the diffusive interfaces spawns the merger of adjoining convection layers, until the cylinder is enveloped in a single bottom layer. With decreasing N, fewer layers form around the cylinder and merger occurs more rapidly. For $N \approx 1$, formation is restricted to a single bottom layer.

For all values of N, convection layer development above the cylinder is driven by vertical heat flow from the bottom layer. Multiple layers form in this manner, with adjoining layers separated by a diffusive interface. However, as is characteristic of double-diffusive convection, subsequent erosion of the interfaces contributes to an ever expanding, contiguous convection layer.

Either initially (for small N) or subsequently (for large N), flow conditions are characterized by an ascending plume in the bottom convection layer. Since upflow is restricted by the diffusive interface separating the bottom layer from the overlying convection (or stable) region, the plume induces a recirculating flow in the convection layer. However, plume impingement on the interface enhances its degradation, fostering the intrusion of warm, salty fluid into the overlying, cooler, less salty layer. This process results in the merger of adjacent convection layers and the establishment of a new interface at a higher vertical location. The process repeats itself, providing an important distinction between convection layer development in solutally and thermally stratified media. Namely, steady-state conditions for double-diffusive convection are attained only when counter thermal and solutal effects cease to exist. In essence, this condition occurs when the plume reaches the free surface and there is thermal convection of well-mixed salty water. In contrast, thermal plumes impeded by a thermally stratified medium can attain a steady, equilibrium height for which continued growth does not occur [5–7].

For large N, the initial confinement of convection to layers adjoining the cylinder limits the ability to reject heat to overlying non-convecting (or convecting) layers. Hence, Nusselt numbers are well below those associated with natural convection in an unstratified, infinite medium. However, with decreasing N and/or increasing time, the merger of adjoining convection layers and plume development above the cylinder allow the Nusselt number to approach the limiting result for an unstratified, infinite medium. The limit is reached for a plume height of approximately two cylinder diameters.

Acknowledgement—Support of this work was provided by the National Science Foundation under Grant No. CBT-8316580.

REFERENCES

1. J. S. Turner, Multicomponent convection. In *Annual Review of Fluid Mechanics* (Edited by M. VanDyke, J. V. Wehausen and J. L. Lumley), Vol. 17, pp. 11–44. Annual Reviews, Inc., Palo Alto, California (1985).
2. S. Ostrach, Fluid mechanics in crystal growth—The 1982 Freeman Scholar Lecture, *J. Fluids Engng* **105**, 5–20 (1983).
3. T. Carlberg, The effect of convection upon off-eutectic composite growth of Al–Cu alloys, *J. Crystal Growth* **66**, 106–120 (1984).
4. F. P. Incropera, Buoyancy effects in double-diffusive and mixed convection flows, *Proc. 8th Int. Heat Transfer Conf.*, Vol. 1, pp. 121–130 (1986).
5. R. A. Wirtz and C. M. Chiu, Laminar thermal plume rise in a thermally stratified environment, *Int. J. Heat Mass Transfer* **17**, 323–329 (1974).
6. K. E. Torrance, Natural convection in thermally stratified enclosures with localized heating from below, *J. Fluid Mech.* **95**(3), 477–495 (1979).
7. R. Eichhorn, J. H. Lienhard and C.-C. Chen, Natural convection from isothermal spheres and cylinders immersed in a stratified fluid, *Proc. 5th Int. Heat Transfer Conf.*, NC 1.3, pp. 10–14 (1974).
8. W. T. Lewis, F. P. Incropera and R. Viskanta, Interferometric study of stable salinity gradients heated from below or cooled from above, *J. Fluid Mech.* **116**, 411–430 (1982).
9. T. L. Bergman, A. Ungan, F. P. Incropera and R. Viskanta, Mixed layer development in a salt-stratified solution destabilized by a discrete heat source, *J. Heat Transfer* (1987), in press.
10. T. L. Bergman and A. Ungan, Experimental and numerical investigation of double-diffusive convection induced by a discrete heat source, *Int. J. Heat Mass Transfer* **29**, 1695–1709 (1986).
11. Yu. D. Chashechkin and V. S. Tupitsyn, Structure of free convective flow above a point source of heat in a stratified liquid, *Sov. Phys. Dokl.* **24**, 862–864 (1979).
12. V. S. Tupitsyn and Yu. D. Chashechkin, Free convection above a point source of heat in a stratified fluid, *Izv. Akad. Nauk. SSSR, Mekh. Zhid. i Gaza* **2**, 27–36 (1981).
13. A. B. Tsinober, Y. Yahalom and D. J. Shlien, A point source of heat in a stable salinity gradient, *J. Fluid Mech.* **135**, 199–217 (1983).
14. H. E. Huppert, R. C. Kerr and M. A. Hallworth, Heating or cooling a stable compositional gradient from the side, *Int. J. Heat Mass Transfer* **27**, 1395–1401 (1984).
15. B. Gebhart and R. H. Hubbell, Transport processes induced by a heated horizontal cylinder submerged in quiescent salt-stratified water, *Proc. 24th Heat Transfer and Fluid Mechanics Institute*, pp. 203–219 (1974).
16. Yu. D. Chaschechkin and V. A. Popov, The structure of free convective flow above a heated cylinder in a stratified liquid, *Sov. Phys. Dokl.* **24**, 827–828 (1979).
17. United States Office of Saline Water, Technical Data Book (1964).
18. F. P. Incropera and M. A. Yaghoubi, Buoyancy driven flows originating from heated cylinders submerged in a finite water layer, *Int. J. Heat Mass Transfer* **23**, 269–278 (1980).
19. V. T. Morgan, The overall convective heat transfer from smooth circular cylinders. In *Advances in Heat Transfer* (Edited by T. F. Irvine and J. P. Hartnett), Vol. 11, pp. 199–264. Academic Press, New York (1975).

ECOULEMENT DOUBLEMENT DIFFUSIF ET TRANSFERT THERMIQUE POUR UNE SOURCE CYLINDRIQUE IMMERGEE DANS UNE SOLUTION SALINE STRATIFIEE

Résumé—On étudie expérimentalement la nature des écoulements doublement diffusifs induits par un cylindre horizontal chaud immergé dans une solution saline stratifiée. Les conditions d' écoulement dépendent fortement du paramètre de stratification N qui mesure le degré initial de stratification stable relativement aux effets thermiques destabilisants. Pour un grand N, l'écoulement est initialement composé de multiples couches de recirculation qui existent autour et au dessous de la source de chaleur et qui sont séparées par des interfaces diffusifs. Quand le temps augmente, les interfaces s'érodent, causant la disparition des couches fluides et l'enveloppement de la source thermique par une couche unique. Quand N diminue, ou dans les dernière étapes d'une expérience avec un grand N, les conditions sont fortement influencées par le développement d'un panache au dessus du cylindre. La couche convective autour du cylindre est pilotée par le panache qui augmente aussi la dégradation de l'interface diffusif séparant la couche du fluide environnant. Pour toutes les valeurs de N, les conditions permanentes sont seulement atteintes après que le panache pénètre la surface libre et l'établissement d'une concentration uniforme en sel élimine l'existence des effets doublement diffusifs. Pour un temps fixé, le nombre de Nusselt moyen pour le cylindre diminue quand N augmente. Néanmoins quelquesoit N, le nombre de Nusselt augmente avec le temps jusqu'à la valeur limite associée à la convection naturelle dans un milieu infini non stratifié.

DOPPELTDIFFUSIVE STRÖMUNG UND WÄRMEÜBERGANG FÜR EINE ZYLINDRISCHE QUELLE, EINGETAUCHT IN EINE SALZLÖSUNG MIT KONZENTRATIONSSCHICHTUNG

Zusammenfassung—Eine experimentelle Untersuchung wurde durchgeführt, um die Beschaffenheit der doppeltdiffusiven Strömung, verursacht durch einen beheizten horizontalen Zylinder, der in eine Salzlösung mit Konzentrationsschichtung eingetaucht ist, zu beschreiben. Die Strömungsbedingungen sind stark abhängig vom Schichtungsparameter N, einem Maß für den ursprünglich stabilen Lösungskonzentrationsverlauf relativ zu den destabilisierenden thermischen Effekten. Für große Werte von N ist die Strömung ursprünglich begrenzt auf mehrfache umlaufende Flüssigkeitsschichten, die in der Umgebung der Wärmequelle vorhanden und durch Grenzflächen voneinander getrennt sind. Im Laufe der Zeit werden die Grenzflächen aufgelöst, verursacht durch Verschmelzung der konvektiven Flüssigkeitsschichten und Umhüllung der Wärmequelle durch eine einzelne Schicht. Mit abnehmendem N oder, in den späteren Stadien eines Experiments mit großem N, werden die Bedingungen stark durch die Entwicklung von Auftriebsfahnen oberhalb des Zylinders beeinflußt. Die Strömung in der konvektiven Schicht um den Zylinder wird durch die Auftriebsfahne gesteuert, welche außerdem die Grenzfläche, welche diese Schicht von dem darüberliegenden Fluid trennt, abbaut. Für alle Werte von N werden stationäre Bedingungen nur erreicht, nachdem die Auftriebsfahne zur freien Oberfläche durchgedrungen ist. Das Zustandekommen einer einheitlichen Salzkonzentration beseitigt das Auftreten von doppeltdiffusiven Effekten. Für eine vorgeschriebene Zeit nimmt die mittlere Nusselt-Zahl für den Zylinder mit wachsendem N ab. Jedoch, unabhängig von N, wächst die Nusselt-Zahl mit der Zeit auf den Grenzwert der freien Konvektion in einem ungeschichteten unendlichen Medium.

ДВОЙНОЕ ДИФФУЗИОННОЕ ТЕЧЕНИЕ И ТЕПЛОПЕРЕНОС В СЛУЧАЕ ЦИЛИНДРИЧЕСКОГО ИСТОЧНИКА ТЕПЛА, ПОГРУЖЕННОГО В СТРАТИФИЦИРОВАННЫЙ РАСТВОР СОЛИ

Аннотация—Выполнено экспериментальное исследование для выяснения природы двойного диффузионного течения, индуцированного нагреваемым горизонтальным цилиндром, погруженным в стратифицированный солевой раствор. Условия течения сильно зависят от параметра стратификации N, который является мерой степени начальной устойчивой стратификации раствора относительно дестабилизирующих термических эффектов. При больших N течение вначале происходит только в многочисленных слоях рециркулирующей жидкости, расположенных вокруг теплового источника и над ним, и разделенных диффузионными поверхностями раздела. С течением времени эти поверхности разрушаются, и конвективные слои жидкости сливаются в один слой вокруг источника тепла. С уменьшением N или при больших N на поздних стадиях эксперимента условия течения в значительной степени определяются развитием свободноконвективной струи над цилиндром. Течение в конвективном слое у цилиндра увлекается этой струей, что приводит к разрушению диффузионной поверхности, отделяющей этот слой от вышележащего объема жидкости. При всех значениях N стационарное состояние устанавливается только после того как свободноконвективная струя достигает свободной поверхности жидкости и установившаяся однородная концентрация соли исключает существование эффектов двойной диффузии. В заданный момент времени среднее число Нуссельта для цилиндра уменьшается с ростом N. Однако, независимо от N, число Нуссельта увеличивается со временем до предельного значения, соответствующего свободной конвекции в нестратифицированной бесконечной среде.